



ORIGINAL ARTICLE OPEN ACCESS

Pareto Optimization of the Integration of Renewables for the Supply of Battery-Electric and Hydrogen-Electric Multiple Units at a Single Site

Stefan Arens¹  | Alexander Windt² | Christoph Streuling³ | Benedikt Hanke¹ 

¹DLR Institute of Networked Energy Systems, Koln, Germany | ²Reiner Lemoine Institute, Neuss, Germany | ³DLR Institute of Vehicle Concepts, Koln, Germany

Correspondence: Stefan Arens (stefan.aren@dlr.de)

Received: 9 February 2024 | **Revised:** 7 November 2024 | **Accepted:** 11 November 2024

Funding: This study was funded by the German Center for Rail Traffic Research (DZSF) at the Federal Railway Authority (EBA), project No. EBA_2020-13-U-1202.

Keywords: battery-electric trains | energy management | fuel cells | hydrogen trains | renewable energy | system sizing | train line supply concepts

ABSTRACT

Battery- and hydrogen-powered trains are emerging technologies that have the potential to play a key role in the decarbonization of railway lines for which full trackside electrification is not feasible. In this study, we examine Pareto-optimal energy supply concepts for a specific location along the Cologne–Gerolstein railway line. We investigate two supply concepts, one for battery trains making use of overhead line islands (OHLIs), referred to as the *OHLI supply concept*, and another for hydrogen trains that make use of hydrogen refueling station (HRSs), referred to as the *HRS supply concept*. The public grid, as well as renewable energy sources such as wind and PV energy, are considered sources of electrical energy supply. The sizing of these takes into account storage technologies and load time series specific to each supply concept. Simulation models are defined to evaluate the characteristics of an OHLI and HRS supply concept located in a small town (Gerolstein, Germany). Our findings indicate that the HRS supply concept results in more than twice the cost per MWh (111%/MWh higher) compared to the OHLI supply concept. However, the HRS supply concept achieves a 24.7% higher degree of self-sufficiency. Furthermore, the HRS supply concept requires a larger energy system in terms of installed renewable power and storage capacity. This enables the HRS to supply the entire line with energy, whereas the OHLI supply concept covers only a share of the overall energy demand of battery trains at the location under consideration. The remaining energy demand is covered by existing overhead lines or OHLI at another location.

1 | Introduction

The railway system represents a transport mode that can make a significant contribution to meeting future mobility needs through high efficiency and safety standards. However, on non-electrified routes with low traffic volumes, local passenger transport often relies on hydrocarbon-based fuel sources [1]. To

achieve further decarbonization of the rail sector, it is necessary to introduce alternatives on routes on which full electrification is neither possible nor economically viable.

Two types of multiple-unit train systems are being considered as potential replacements for fossil fuel-based train systems (primarily diesel trains), where electrification of the entire line

Acronyms: BEMU, battery-electric multiple unit; CAPEX, capital expenditures; CO₂-eq, carbon dioxide equivalent; DMU, diesel multiple unit; HEMU, hydrogen-electric multiple unit; HRS, hydrogen refueling station; HVAC, heating, ventilation, and air conditioning; MO, multi-objective optimization; OHLI, overhead line island; OPEX_o, Operational expenditures; PV, photovoltaic; PVS, photovoltaic system; SMOOTHs, Simulation Model for Optimized Operation and Topology of Hybrid Energy Systems; TPTt, trajectory planning tool; WT, wind turbine.

This is an open access article under the terms of the [Creative Commons Attribution](https://creativecommons.org/licenses/by/4.0/) License, which permits use, distribution and reproduction in any medium, provided the original work is properly cited.

© 2025 The Author(s). *Energy Science & Engineering* published by Society of Chemical Industry and John Wiley & Sons Ltd.

is not possible or not feasible: hydrogen–electric multiple units (HEMUs) and battery-electric multiple units (BEMUs) [2]. The multiple-unit train systems differ in terms of energy efficiency, operational range, and energy supply concepts. BEMUs can be operated with higher efficiencies due to their technological characteristics [3]. However, they generally have shorter operational ranges than HEMUs, which have ranges that allow for operation for well above 10 h [4], while achieving an operational range of up to 1000 km [5, 6]. For BEMUs, the operational range lies at about 80–100 km [5, 7]. Note that the operational range depends on the battery, fuel cell, and hydrogen vessel capacity, as well as the operation profile, train specifications, and other impacting factors. The energy supply concept for BEMUs requires the provision of electrical energy to charge the respective batteries and HEMUs require hydrogen, a chemical energy carrier.

A BEMU typically draws the traction energy required for movement and auxiliaries during operation from the overhead line or an installed battery. The overhead line can be fed from the traction energy supply or from a decentralized rail energy supply. A central rail energy supply utilizes the railroad energy supply network. If this is not available, overhead line island (OHLI) systems can be installed, which require a connection to the public electricity grid, constituting a decentralized system. An OHLI consists of an overhead line and a feeding substation that is erected only on a portion of the route between the departure and destination of a multiple unit. The OHLI can be positioned along the route or situated at the end stations depending on the route's topology and operational requirements [8], as well as at night depots, comparable to bus depot stations.

Typically, less than 10 km of overhead line are erected for a single OHLI. If there is a BEMU beneath it, it can recharge the traction battery or use the energy for traction energy demand or auxiliaries, depending on the energy management of the BEMU. In sections without overhead lines, the BEMU's energy demands must be met by battery storage. The energy supply for BEMUs, using OHLI, is denoted as an OHLI supply concept in this study.

To buffer the demand profile at an OHLI, a stationary battery storage can be installed, whereas the cost significantly varies. While Maheswari et al. [9] describes cost ranging from 750 to 2200 €/kWh, in [10], the energy system cost of lithium-ion phosphate batteries are given as 510–356 \$/kWh, depending on the battery size. The efficiency of a lithium-ion battery cell can reach 97.3% [11]. However, additional components such as DC–DC converter reduce the overall system efficiency. The round trip efficiency from AC to AC lies around 85% [12]. Batteries are applied in varying sizes, depending on the use case. Self-consumption of energy used relatively low battery capacities up to 100 kWh, whereas for renewable integration battery capacities up to 1000 kWh are installed [13]. However, batteries are also applied for storage applications in the MWh range [11].

The HEMU uses fuel cells to convert hydrogen into electrical energy, which then powers the electric engines of the respective train. The hydrogen that is used as a fuel for HEMUs can either be stored in a liquid or gaseous state. The vehicle storage system, as well as the hydrogen refueling station (HRS), must be

adapted to the specific hydrogen state in use. It was assumed that the HEMUs consist of a storage tank operating at 350 bar. The HRS provides hydrogen to a HEMU; in general, it consists of a storage tank and fluid conveying device [6].

The energy supply for HEMUs, using an HRS, is denoted as an HRS supply concept in this paper.

Fuel cells are a critical part of the HRS supply system. They are available for different power ranges, from the kW range to the MW range [14, 15]. Compared with batteries, fuel cells exhibit advantages in refueling time and energy density. However, the cost is higher and the efficiency is lower [16]. The electric efficiency of a fuel cell can reach up to 70%, where an electric efficiency of 40% is more common. To further increase the efficiency, the fuel cell can be used in a combined heat and power mode, boosting the efficiency up to 95% [15]. The cost of fuel cells varies significantly, ranging from 3000 €/kW [15] to 100,000 €/kW [17].

In general, the integration of renewable generation technology shows great potential for system optimization [18]. Therefore, the utilization of locally-available renewable energy sources for the energy supply of OHLI and HRS supply concepts can be considered advantageous from technical and economic perspectives. One technical consideration is the reduction of transmission losses, while an economic one includes cost reduction through self-generated power and reduced reliance on purchasing energy from the electricity grid [19]. Furthermore, the integration of renewable generation can mitigate CO₂-eq emissions [8, 18].

A comparison between batteries and hydrogen for rail application was performed in [20], focusing on the challenges arising due to demand and not considering the supply side. In the supply context, the coupling of railway operation and renewable energy generation offers great potential, as demonstrated for a region in northeast Germany, studying the production of hydrogen to supply HEMU [21]. The integration of wind energy systems would also be beneficial for supplying electrical energy to BEMU, as demonstrated for a rail line running from Berlin to Poland [8]. However, the sizing of OHLI and HRS supply concepts requires further investigation with regard to a comparison of the respective supply concepts and the optimized integration of different energy sources. Sizing the supply is a complex task that involves considering the energy storage and generation capacities of various technologies such as wind energy and PV systems. This task also involves taking into account local weather resources and the characteristics of load time series. Furthermore, the system sizing can be performed with different optimization targets.

Multi-objective optimization (MO) is a technique employed for these problems. The application enables the optimization of two or more contradicting target values. Thus, robust system dimensions can be identified and the influence of the system components on the respective target variables can be described. Possible optimization targets include life cycle costs and the loss of power quality for an energy system with renewable energy sources, batteries, and electric vehicles [22]. Other multi-objective optimizations deal with

CO₂-eq-emissions, annuities and own consumption of district energy systems [23] and the sizing of remote area energy systems containing back-up units [24].

This study examines the integration of renewable energy systems for HEMU and BEMU energy supply at a single site by means of MO. This enables the robust sizing of such systems with respect to conflicting optimization targets, namely local CO₂-eq emissions and cost. The primary research contributions are:

- Pareto-optimal sizing of an energy system for a battery-electric, as well as a hydrogen-based supply concept for a single location based on a case study in Gerolstein.
- Comparative evaluation of the advantages and disadvantages of hydrogen and battery-electric train supply concepts from a single location perspective.

This paper is organized as follows: Section 2 describes the methodology used. This includes the system dimension optimization approach as well as the operation optimization for the OHLI and HRS supply concept. Section 3 describes the results of the case study on a per-supply concept on a single side. The load and renewable generation time series required for modeling are introduced and the Pareto fronts are described to analyze the supply concept characteristics for the optimization targets cost and CO₂-eq emissions. Additionally, a system at the center of the Pareto front was selected to serve as an in-depth comparison between both supply concepts, the results of which are discussed. Finally, Section 4 presents the conclusions and outlook.

2 | Optimization Model

The optimization approach for the OHLI and HRS supply concepts is illustrated in Figure 1. The optimization is based on a sizing optimization and an operation optimization. Both steps alternate. The sizing optimization algorithm proposes a solution candidate, which represents a system dimensioning (system configuration).

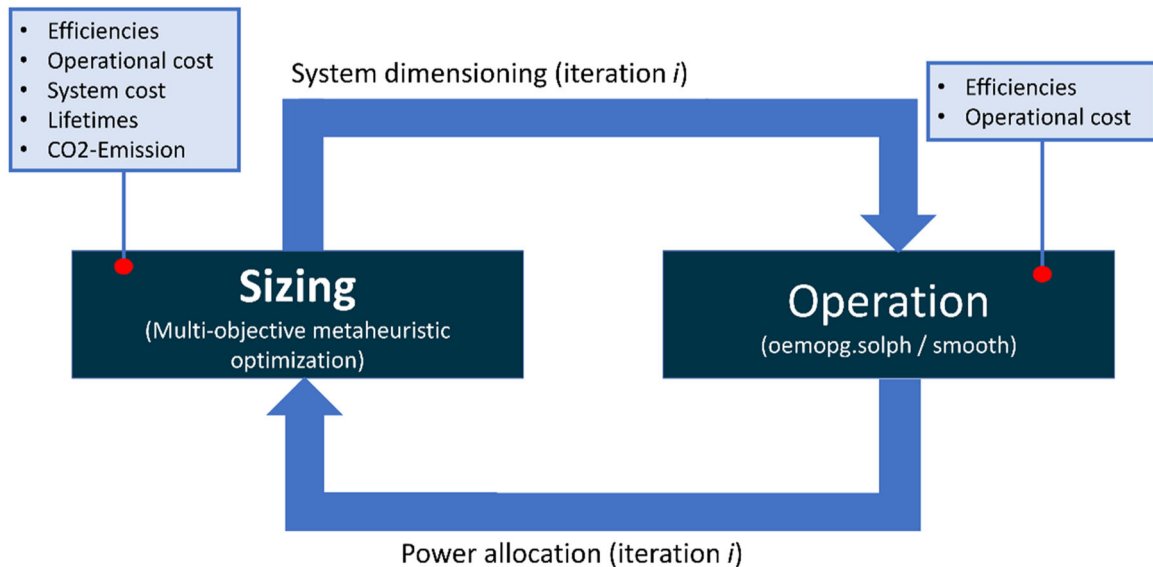


FIGURE 1 | Optimization procedure for the OHLI and HRS supply concepts.

Based on the system sizing, an operational optimization is subsequently carried out to allocate the power profiles of the respective storage capacities, the grid connection and, in the case of the HRS supply concept, the electrolyzer, taking into account the operating costs and efficiencies. The results of the operational optimization and the system sizing are then used for the overall system evaluation.

Following the system's evaluation, new solution candidates are proposed by the optimization algorithm to start another iteration.

2.1 | Sizing

For system sizing, a multi-objective optimization with respect to a cost function $f_{\text{cost}}(x)$ and an emission function $f_{\text{CO}_2\text{-eq}}(x)$ was performed, where x represents a generic input.

$f_{\text{cost}}(x)$ considers the investment, as well as the operation and variable cost. Operations and variable costs are calculated based on a constant yearly value for each system component. The investment cost for a system component s is integrated by annuities, as per the following Equation:

$$a_s = \text{CAPEX}_s \frac{r \cdot (1 + r)^{L_s}}{(1 + r)^{L_s} - 1}. \quad (1)$$

CAPEX _{s} refers to the capital expenditure of the system component s , L_s its lifetime, and r the interest rate.

$f_{\text{CO}_2\text{-eq}}(x)$ considers the emissions during operation or construction, depending on the system component. Emissions during operation are summed over the period of 1 year. Emissions during construction are then determined and divided by the lifetime of the system components. Therefore, $f_{\text{cost}}(x)$ and $f_{\text{CO}_2\text{-eq}}(x)$ refer to a 1-year period.

The optimization was carried out for both the OHLI and HRS supply concepts. Each supply concept consists of a grid

connection, which acts as a backup for time intervals without sufficient generation from renewables and to feed in excess generation. However, the decision vector x differs due to different components for the respective concepts.

Equation 2 describes the variables for the optimization of the OHLI supply concept:

$$x_{\text{OHLI}} = (I_{\text{PV}}, I_{\text{wind}}, C_{\text{battery}}), \quad (2)$$

where I_{PV} describes the number of PV systems, I_{wind} the number of wind energy systems, and C_{battery} the battery capacity. The number of renewables is discretized to account for the scaling of small-scale systems, for example, due to string inverters and the power output of single wind turbines (WTs). The battery capacity is considered less dependent on discretization as a modular approach and is fairly common. Furthermore, the costs are modeled depending on the capacity according to data from [10]. This approach offers a balance between realism and practicality. The elements of the OHLI supply system are depicted in Figure 2.

Equation 3 describes the variables for the optimization of the HRS supply concept:

$$x_{\text{HRS}} = (P_{\text{nom-PV}}, P_{\text{nom-wind}}, C_{\text{H}_2\text{storage}}, P_{\text{nom-ely}}), \quad (3)$$

where $P_{\text{nom-PV}}$ describes the nominal power of PVS, $P_{\text{nom-wind}}$ the nominal power of wind energy systems, $C_{\text{H}_2\text{storage}}$ the capacity of the hydrogen storage, and $P_{\text{nom-ely}}$ the nominal power of the electrolyzer. The elements of the HRS supply concept are modeled with continuous values, as the system design is tailored for significantly higher power levels. Therefore, the limitations in scaling a system with discretized elements are less relevant compared to the OHLI supply concept. The system elements of the HRS supply system are depicted in Figure 3.

Table 1 lists the parameters for the WT, PVS, electrolyzer, and the respective storage technologies for the OHLI and HRS supply concepts. The cost parameters are divided into

capital expenditures (CAPEX) and operational expenditures (OPEX).

2.2 | Operation

The operation optimization for the OHLI supply concept is based on *oemof.solph* [37]. *Oemof.solph* models the energy system by generic components, namely: sinks, sources, buses, and transformers.

For the OHLI supply concept, the generic *oemof.solph* components are used. The time series for the renewables are integrated as sources, as a flow with fixed values for each interval. The two sources (WT and PVS) are connected to a bus, which represents a supply source. Furthermore, a source and a sink are assigned to this bus, which represents the grid connection. Both elements integrate flows that are variable in power, with the source having as cost the price of energy, and the sink the negative feed-in tariff. The supply bus is connected by a transformer to the battery bus. The transformer is parameterized with a constant efficiency to represent the AC-DC converter. A battery is connected to the battery bus, which is modeled by generic storage. The battery bus is then connected to a load bus via another transformer, which is also parameterized with a constant efficiency. This transformer represents the DC-AC converter. Finally, the load time series of the OHLI is connected to the load bus in the form of a sink, with fixed values over the optimization period. The time period for the optimization is 1 year, which is resolved in 10-min intervals.

The modular simulation framework, “Simulation Model for Optimized Operation and Topology of Hybrid Energy Systems” (SMOOTH), was used to model the HRS supply concept [30]. SMOOTH enables the nonlinear, multi-modal modeling of technical components such as WT, PVS, battery storage, and electrolyzers, as well as entire energy systems. The simulation is time step-resolved. For each time step, an *oemof.solph* model for the HRS supply concept is set up and solved. The simulation is carried out for 1 year, as in the

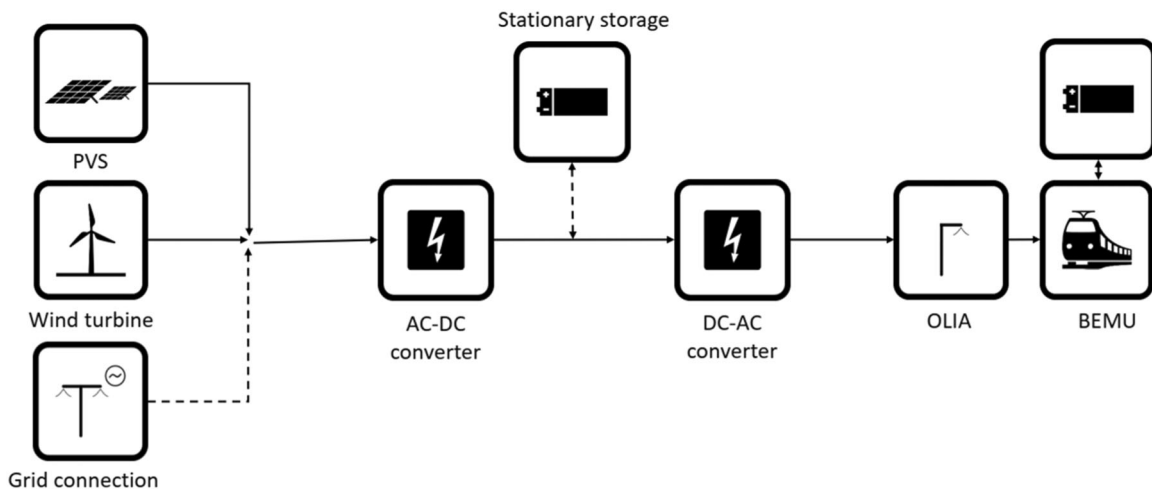


FIGURE 2 | System morphology of the OHLI supply concept. The electricity sources are the grid connection, wind and PVS; the battery storage acts as a buffer; the OHLI serves as the load.

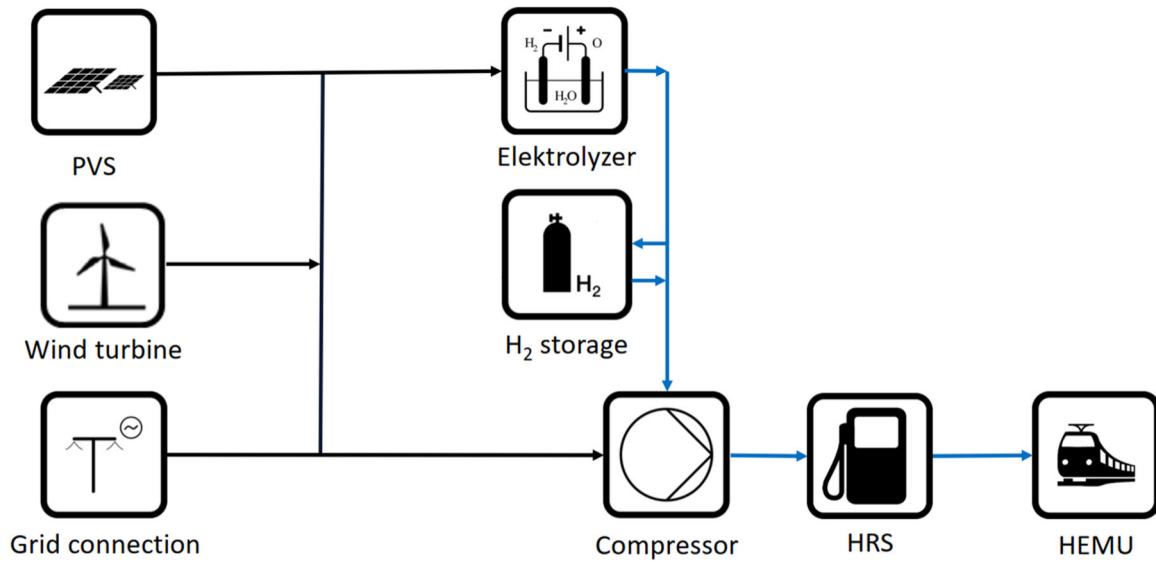


FIGURE 3 | HRS supply concept. The electricity sources are the grid connection, wind, and PVS; the hydrogen source is an electrolyzer; the storage acts as a buffer; the compressor and subsequent HRS serve as the loads.

TABLE 1 | Parameters for optimizing the OHLI and HRS supply concepts.

Parameter	Parameter value	Source
Price of energy from grid [€/kWh]	0.1855	[25]
Feed in tariff [€/kWh]	-0.05	[26–28]
CAPEX WT [€/kW _{installed}]	1750	[29]
OPEX WT [€/kW _{installed}]	30	[30]
CAPEX PVS [€/kW _{peak}]	900	[29]
OPEX PVS [% of CAPEX PVS]	2.5	[30]
Lifetime PVS [a]	25	[31]
Lifetime WT [a]	25	[32]
Lifetime battery [a]	10	[10]
CO ₂ PVS [g/kWh _{produced}]	48	[33]
CO ₂ WT [g/kWh _{produced}]	11	[33]
CO ₂ battery [g/kWh _{installed}]	158	[34]
CO ₂ grid consumption [g/kWh]	366	[35]
CO ₂ electrolyzer [g/kgH ₂ _{produced}]	31.7	[36]
Interest rate [%]	3	Assumed

case of the OHLI supply concept; however, the intervals are at a 1-h resolution.

3 | Case Study

The case study was performed using the example of the regional rail route Cologne–Trier, which is currently served by multiple diesel units. The feasibility of an operation utilizing BEMU and HEMU, including scenarios for HRS and OHLI supply concepts, has also been investigated.

Figure 4 displays the route location and operated rail lines (based on timetable year 2021). The full route has a length of 180.1 km, with 11.8 km starting from Cologne and 6.5 km starting from

Trier, being equipped with an overhead line. The HRS and OHLI sites for the BEMU and HEMU scenarios were set to the location of Gerolstein, which is also the terminus station of the RB24 line. The distance between Cologne and Gerolstein accounts for a length of 111.6 km. The lines Cologne–Trier (RE12/RE22) and Cologne–Gerolstein (RB24) are operated at a service frequency of about 30, as given by the timetable [38].

3.1 | Energy Demand of BEMU and HEMU

A generic multiple unit was used to model the energy demand for the BEMU and HEMU alternatives. The current regional rail service with diesel multiple units (DEMU) along the respective

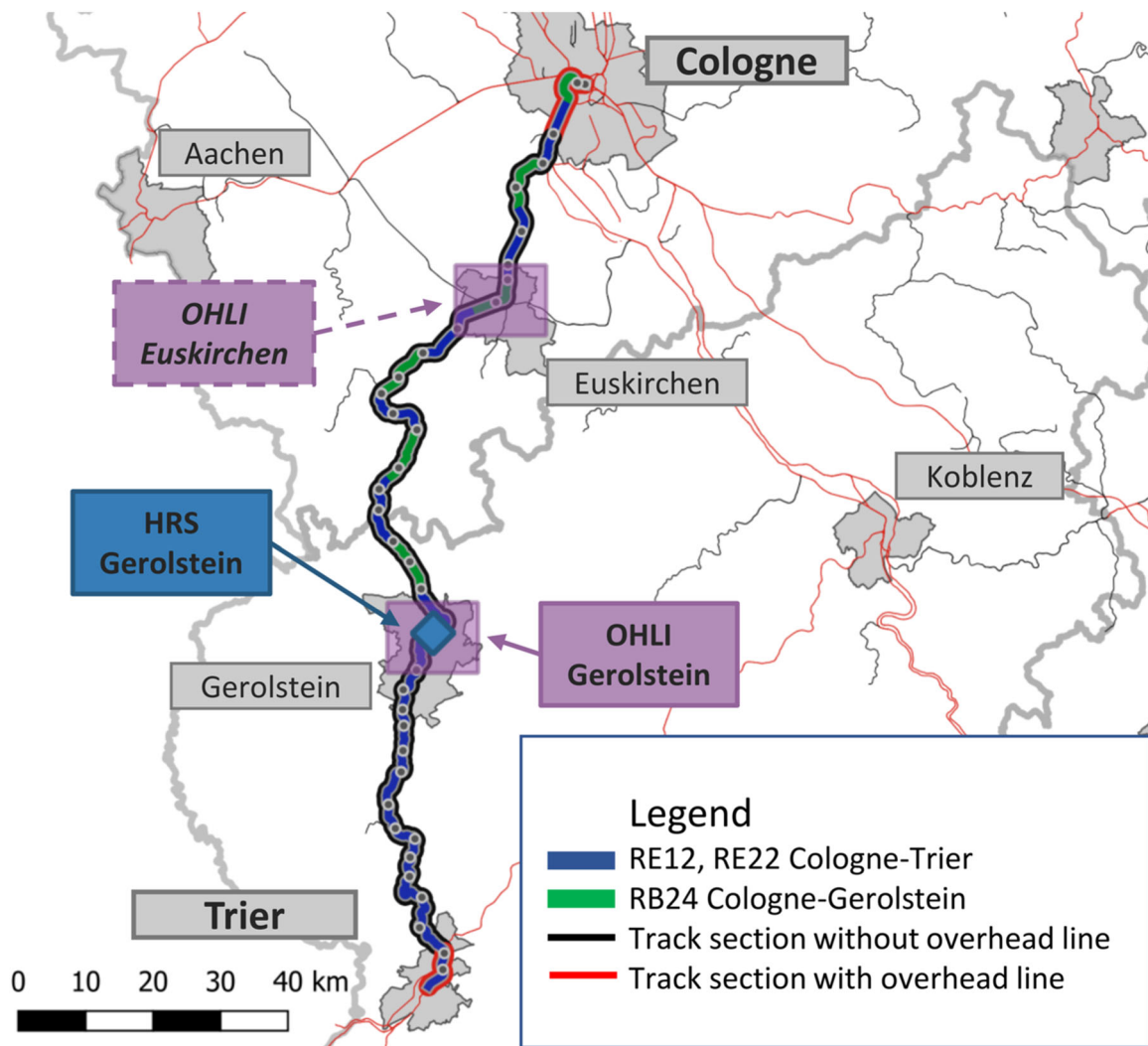


FIGURE 4 | Lines that serve as a basis for the demand time series, modeling the railway track between Cologne and Trier (based on regional rail transport service in 2021). The blue line describes the route from Trier to Cologne and the line with green sections the route from Gerolstein to Cologne. The thin red and black contours of the thick lines mark the electrification status of the respective route section.

lines involves different two- and three-car multiple units. As a simplification, BEMU and HEMU energy demand simulations of all lines were carried out based on a two-car multiple. The specifications of the two-car multiple unit with a Jacobs bogie are summarized in Table 2. The energy demand at BEMU's pantograph for one single rotation is 967 kWh, assuming a normal day, and 1371 kWh for a design day with increased heating ventilation and air conditioning (HVAC) demand.

It is assumed that an OHLI will be built at Gerolstein to charge the BEMUs in the context of the OHLI supply concept. For the hydrogen supply concept, a hydrogen refueling station is assumed to be built at Gerolstein to supply the hydrogen-electric multiple units.

The DLR Trajectory Planning Tool (TPT) presented in [39], was used to model the energy demand of the multiple units. Given the train specifications and route characteristics (timetable, route, and elevation profiles, speed limits), a speed trajectory and the associated power required at the wheel were determined by longitudinal dynamic simulation. The driving profile is composed of acceleration and deceleration phases, as well as phases with constant speed.

TABLE 2 | Specifications of the two-car multiple-unit.

Parameter	Parameter value
Train length [m]	42
Train empty mass [t]	95
Train number of seats [1]	120
Max. traction power [kW]	1200
Max. velocity [km/h]	140
P_{HVAC} normal case [kW]	21.4
Max. P_{HVAC} (design case) [kW]	78.4

The total train energy demand was calculated based on the energy demand at the traction motors. Depending on the powertrain architecture, that is, fuel cell-, hybrid-, or battery-electric, the relevant efficiencies of the components are set based on [39]. The power demand of auxiliaries takes the consumption of HVAC and traction cooling into account. The load time series for the design case refers to increased HVAC demand due to more extreme climatic conditions in terms of

ambient temperatures (assumption). The normal case considers average HVAC loads, which were calculated based on the approach of [40] using average monthly air temperatures in Germany according to [41].

Taking into account the power requirements for auxiliaries and for traction, the total energy demand was calculated at each time step. The TPT models the movement and traction energy demand of a respective train at a 1-s resolution. A simplified model was designed to model the energy management strategy for the fuel cell- and battery-electric powertrain setups. The energy management model includes recuperation of braking energy at times when the battery is not fully charged.

In the case of the BEMU, the energy demand, which is covered via pantograph from the overhead line on the OHLI, acts as the system boundary. The maximum recharging power during standstill is set to 1.2 MW for a 15 kV overhead line system, which refers to a current of 80 A at the pantograph, according to limitations given by the normative framework (DIN EN 50367) [42]. While the train is in motion, we assumed a maximum power of 1.8 MW during the trip per BEMU.

The BEMU battery capacity has been set to 670 kWh, based on an iterative approach considering the energy demand in the design case and by limiting the minimum state of charge of the battery system during operation.

The modeling of the HEMU hydrogen demand is based on an integrated energy model, assuming a 400 kW fuel cell and battery storage, which covers additional power demand, especially during the acceleration phases.

For BEMU, the power demand at the overhead line acts as the system boundary, and for HEMU, the hydrogen demand at the fuel fill neck is defined as the demand time series system boundary.

Table 3 shows the BEMU and HEMU energy demand characteristics for a round trip operating on the rail line Cologne–Trier and the related partial lines, both for the design and normal case.

The length of the round trip and the electrical BEMU energy demand do not correlate directly, as only a portion of the energy is recharged at the Gerolstein OLIA. The share is significantly influenced by the recharging time and differs depending on whether the OHLI is located at the start/terminus station or along the route.

TABLE 3 | Rotations length and respective energy demands for BEMU and HEMU round trips at OHLI and HRS Gerolstein for the different train services.

Parameter	Case	Cologne–Trier	Cologne–Gerolstein	Gerolstein–Trier
Length [km]	Both	360	222	137
BEMU [kWh(el.)]	Normal	186	197	157
BEMU [kWh(el.)]	Design	280	366	260
HEMU [kg(H ₂)]	Normal	51.5	36.4	16.7
HEMU [kg (H ₂)]	Design	72.4	50.0	24.2

The discussed daily service profiles (given by the service operator DB Regio) include all trips in both directions (Gerolstein–Trier, Gerolstein–Cologne) and are carried out with different two- and three-car DMUs (Alstom Lint 81 and Lint 54, Bombardier Talent). During the study there have been only a limited number of 2-car BEMUs available to the market. As a simplification, we modeled two-car DMUs based on the abovementioned specifications of a two-car generic multiple unit, which is shorter than the state of the art DMUs. The 3-car DMUs (train length of 81 m) are modeled by two coupled generic 2-car multiple unit (2 × 42 m), accounting for the increased energy and power demands.

The double traction of multiple units has been considered in the BEMU and HEMU scenarios, which results in additional power and energy demands.

In the BEMU scenario, double traction leads to doubled power requirements due to the parallel recharging of each multiple unit (i.e., one pantograph per multiple unit). The actual power demand of BEMU and thus the power requirement at the charging substation depends on the number of BEMUs recharged simultaneously and the BEMU's powertrain specifications (i.e., transformer, battery system power) and the overhead line system (voltage level, current carrying capacity).

Regarding the HEMU scenario, the same assumptions regarding the trips in double traction given by the daily service profile have been made which results in an increased overall hydrogen demand and an increased number of refuelings.

3.2 | Modeled Time Series

The modeling is based on load time series and renewable generation time series. Depending on the supply concept, the load time series differ significantly, whereas the basic renewable generation time series is identical for both supply concepts. As the time series are of critical importance to the simulation results, their modeling is described in detail. The location under investigation here is Gerolstein.

3.2.1 | Load Time Series

The load time series in this study are based on the dynamic modeling of the BEMU und HEMU energy demand with the example of the Cologne–Trier route.

For this study, the two concepts differ with respect to the temporal resolutions of the optimizations and coverage of the route energy demand that were carried out. The BEMU load time series of a respective supply concept is composed of all trains that stop at the OHLI Gerolstein over 1 day. In the OHLI supply concept, an interval length of 10 min was selected for optimization to represent the temporal dynamics of the load time series, which were calculated by the train energy simulation, while keeping the calculation effort reasonable. The load time series for the OHLI supply concept of one example day is shown in Figure 5.

Furthermore, it should be noted that the OHLI in Gerolstein only covers part of the total energy demand of the line. The remaining energy demand is provided by the existing electrification at the starting point, the terminus stations, and another OHLI.

In the HRS supply concept, an interval length of 1 h was selected for optimization. The HRS supply concept covers the entire hydrogen demand of all HEMU running on the line of an HRS constructed in the vicinity of Gerolstein station. Assuming a rolling operation of each HEMU on the discussed lines, an average hydrogen demand for all hydrogen trains was calculated, which must be provided during each refueling. The load time series for the HRS supply concept for 1 day is shown in Figure 6. Compared to the electrical load time series, displayed in Figure 5, the hydrogen demand time series exhibits less dynamics over the course of a day.

To model the load time series of the OHLI and HRS supply concepts for 1 year, synthetic time series were generated, consisting of a

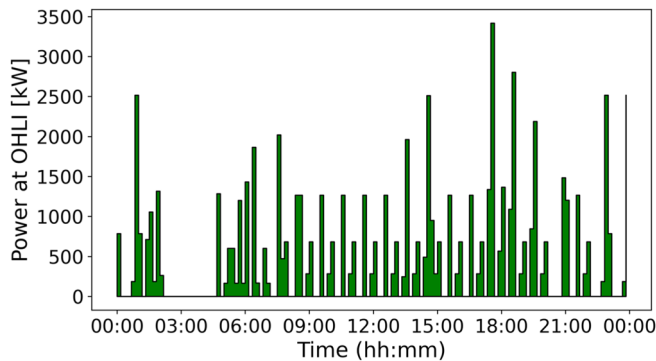


FIGURE 5 | Load time series of the OHLI for one normal day.

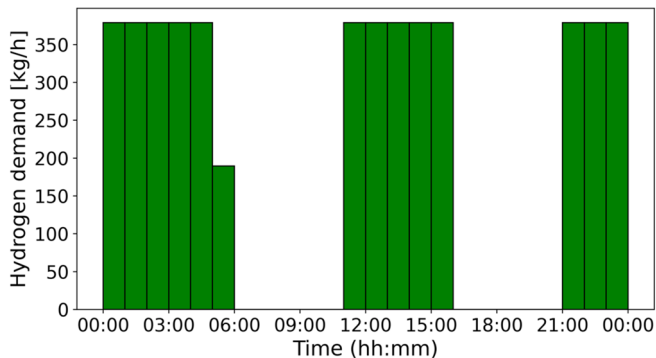


FIGURE 6 | Hydrogen demand at the HRS for one normal day.

normal case and a design case. The design case models an increased demand of multiple units due to operation of the HVAC in challenging weather condition. The design case was integrated for 2 weeks in winter and summer, respectively, when extreme weather conditions prevail. For winter, calendar weeks three and four were selected. During these weeks, low wind and PV resources were available [43]. These conditions pose particular challenges to a renewable-based energy system, as low energy resources are available and low temperatures lead to increased energy demand due to heating. To integrate the design case in summer, the temperature time series of Gerolstein was analyzed. The design case was used for the two consecutive weeks with the highest temperatures.

3.2.2 | Renewable Power Generation

The weather time series for the Gerolstein site, provided by *open_FRED* [44], serve as the basis for the modeling of renewables. The irradiation data, used for PV-modeling, were at 15-min resolution intervals and the wind data, used for wind energy modeling, were at 30-min resolutions.

Electricity generation by a WT was modeled using *windpowerlib* [45]. This software package requires a weather time series and WT type as input parameters. An *Enercon E82/2000* is assumed to be the turbine type, which was modeled with a rotor diameter of 82 m, a nominal power generation of 2000 kW, and a hub height of 108 m.

Generation by a PV system (PVS) was modeled using *pplib* [46]. A *Fronius Symo Advanced 20.0-3 480* was selected as the inverter type and *Hanwha Q.Cells Q.Peak BLK G4.1 290Wp* were selected as the module type. Three strings, with 22 PV modules each, were selected to represent a PVS unit based on [47]. With a peak power of 290 W per module, this results in a peak power of 19.14 kW per PVS unit.

The integration of the renewables differs for the OHLI and HRS supply concepts. The OHLI supply systems discretize renewables electricity generation, allowing only the addition of single WTs and PVS units to account for the general lower power magnitudes. The HRS supply systems require higher electrical power, and therefore the renewable electricity generation is not discretized to reduce the computational complexity.

3.3 | Results

To evaluate the results, the Pareto fronts for the OHLI and HRS supply concepts are described with respect to the sizing of the system components. For both supply concepts, a system configuration that lies in the center of the Pareto front were compared to each other. The system configurations were thus compromised between a system configuration with the lowest costs and a system configuration with the lowest CO₂-eq emissions.

Furthermore, a comparative analysis of a single system configuration, which lies in the center of the Pareto fronts of the respective supply concepts, is presented.

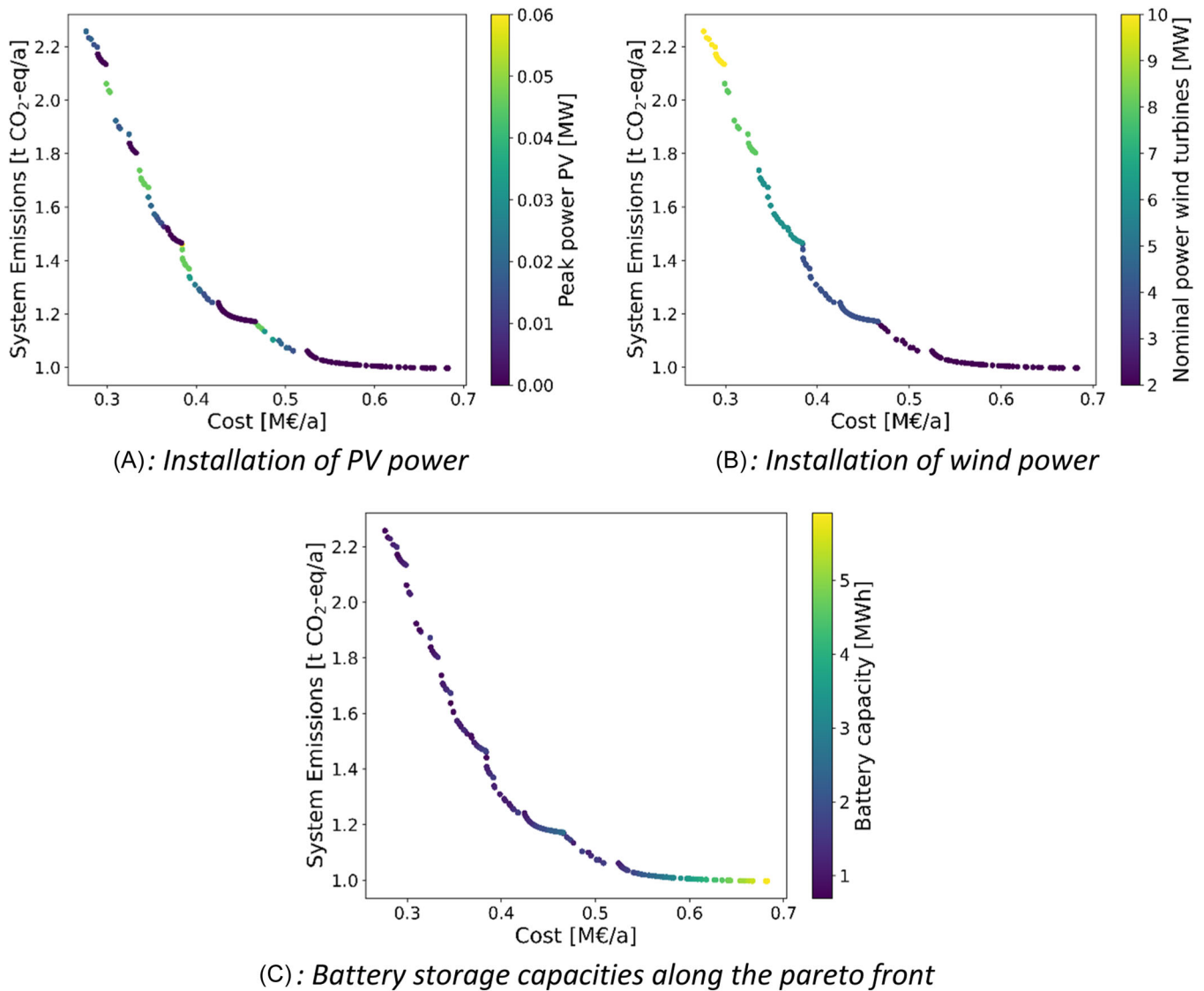


FIGURE 7 | Pareto front for the OHLI supply concept. (A) Installation of PV power. (B) Installation of wind power. (C) Battery storage capacities.

3.3.1 | Pareto Front of the OHLI Supply Concept

Figure 7 shows the Pareto front of the OHLI supply concept with respect to the system configurations.

Figure 7A shows the installed nominal powers of PVS along the Pareto front. With regard to PV systems, it can be seen that these were built at the beginning of a wind stage (constant number of wind energy systems), that is, they achieve the lowest values in terms of costs. It can be concluded that PV systems are an instrument for adjusting costs and CO₂-eq emissions within a wind stage.

Figure 7B displays the installed nominal powers of WTs along the Pareto front. It can be seen that the number of WTs (the maximum power per WT is 2000 kW) essentially determines the position of the dimensioning on the Pareto front. Dimensioning with low costs has a high number of WTs. The number then gradually decreases until a single WT is installed. In the following, parts of the Pareto front

that built the same number of WTs, are therefore referred to as the wind stage.

Figure 7C shows the installed battery capacity along the Pareto front. In terms of battery capacity, it can be seen that moderate capacities are used along the entire Pareto front. These therefore represent a sensible addition to integrate renewable energy generation into the system to reduce costs, as well as CO₂-eq emissions. If the Pareto front is examined in the direction of high costs towards minimal CO₂-eq emissions, it becomes apparent that battery capacity is steadily increasing. The local storage is thus used to avoid the purchase of grid electricity, which is parameterized with high CO₂-eq emissions. However, it should be noted that an increasing battery capacity is reflected in strongly increasing costs, whereas the reduction of CO₂-eq emissions is comparatively small. Thus, a reduction in the CO₂-eq emissions from approximately 1000 t/a to approximately 900 t/a represents a CO₂-eq emissions reduction by 10%, whereas the cost increase from 550 k€ to approximately 690 k€ represents an increase in cost by 25%.

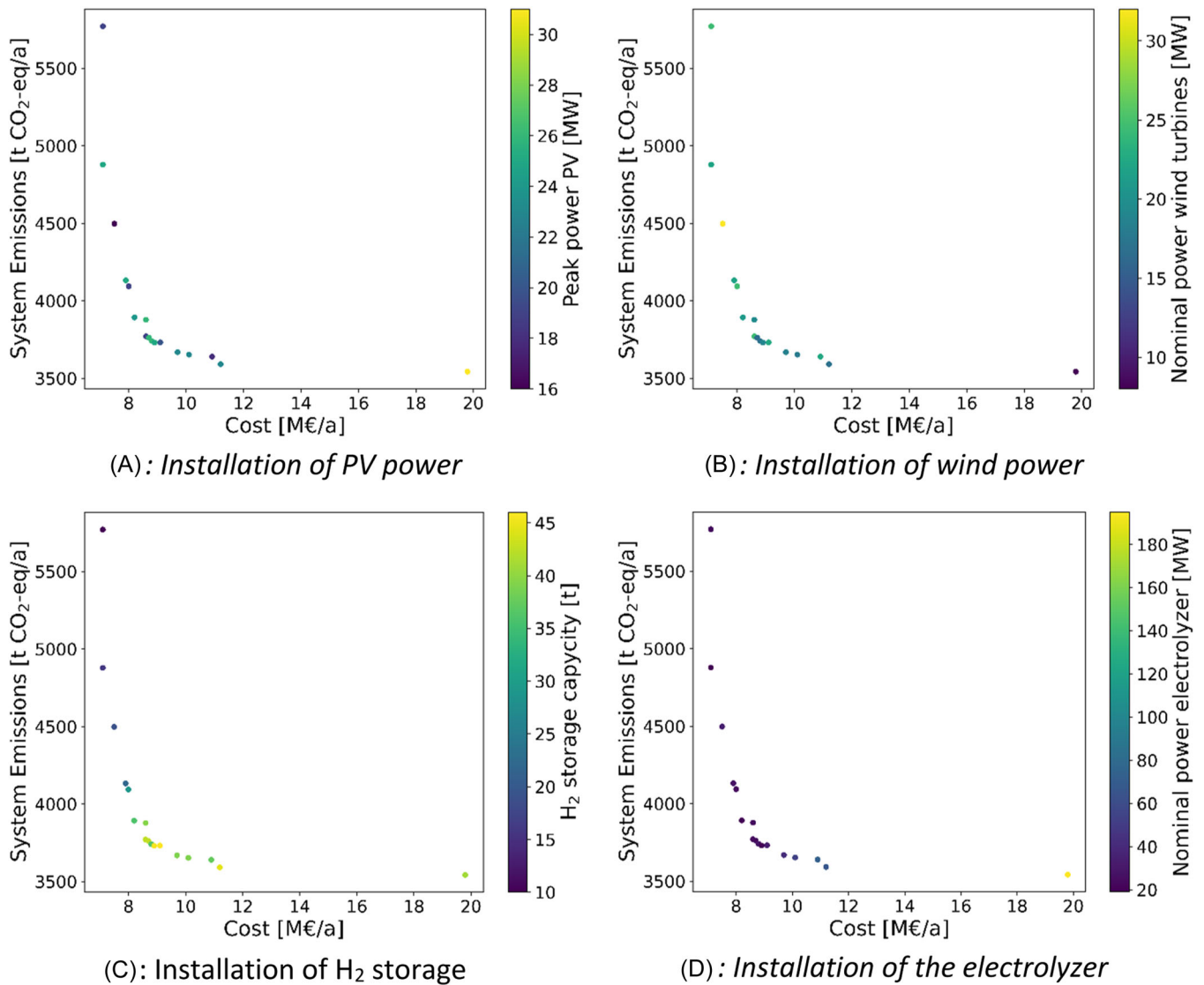


FIGURE 8 | Pareto front for the HRS supply concept. (A) Installation of PV power. (B) Installation of wind power. (C) Installation of H₂ storage. (D) Installation of the electrolyzer.

3.3.2 | Pareto Front of the HRS Supply Concept

Figure 8 shows the Pareto front for the HRS supply system and its system configurations. Due to the significantly increased system complexity, and so the higher computation times, the Pareto front is less populated compared to the OHLI supply concept.

Figure 8A, it can be seen that the CO₂-eq emission minimum is characterized by a PVS with high peak power. All other system configurations are characterized by smaller PVS but do not show a distinct trend of PVS size.

The installed WT power capacities are shown in Figure 8B. It can be seen that in the low cost direction, higher WT power tends to be installed. Furthermore, the system configuration with the lowest CO₂-eq emissions is characterized by the lowest WT power. Overall, a lower dependency of the HRS concept on the installed type of renewable plant is observed, compared to the OHLI supply concept.

Figure 8C shows the installed storage capacities. A clear dependence of CO₂-eq emissions on storage capacity is apparent. The lower the costs, the lower the installed storage capacity is. It should be noted, however, that even at a minimum cost, a storage capacity of about 10 t_{H₂} is installed.

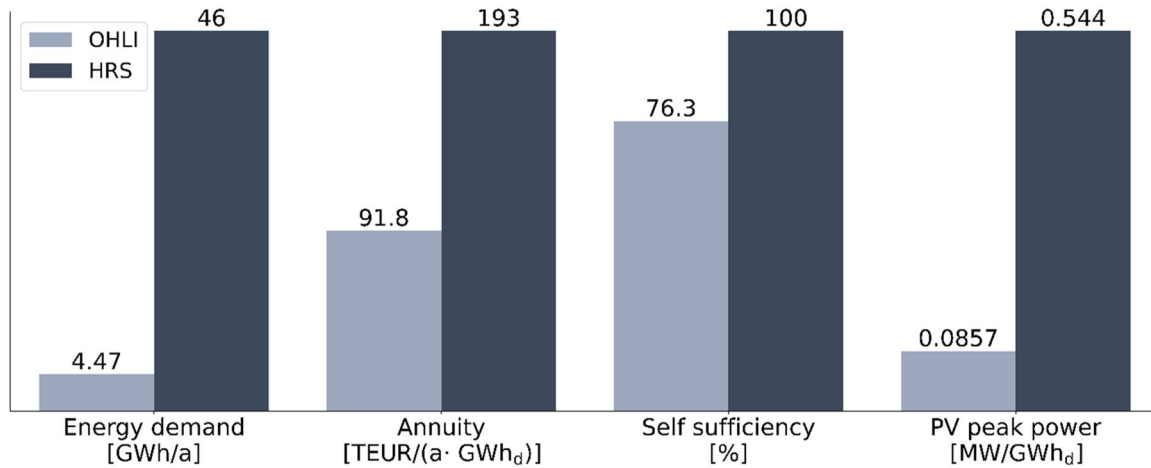
Finally, Figure 8D shows the dimensions of the electrolyzer on the Pareto front. Systems with low costs exhibit lower installed electrolyzer power compared to the CO₂-eq minimum.

3.3.3 | Comparative Analysis

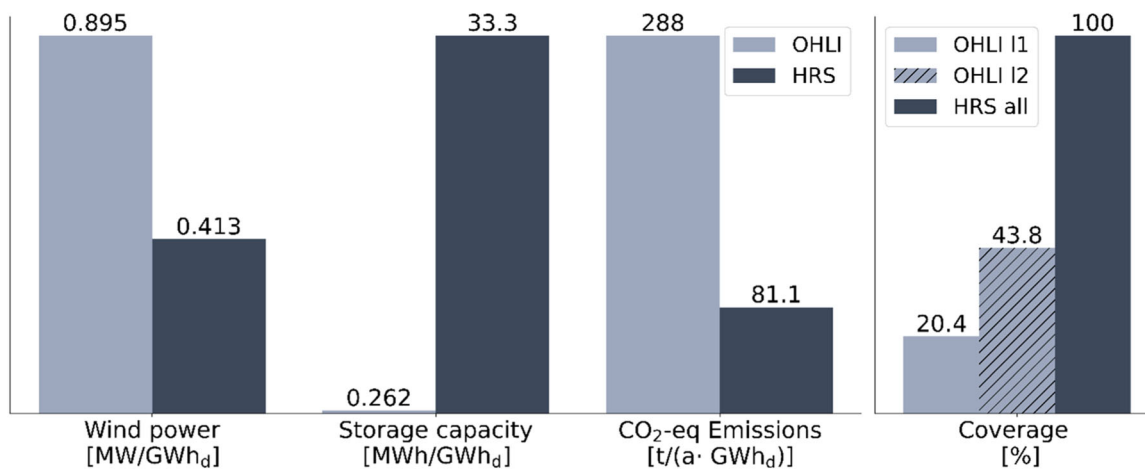
For a comparison of the OHLI and HRS supply concepts, a solution lies in the center of the Pareto fronts between the minimal cost solution and the minimal CO₂-eq emissions solution for each supply concept. Table 4 summarizes the system dimensioning and parameters of both systems used for the comparative analysis.

TABLE 4 | System configuration and KPIs for comparative analysis.

Parameter	OHLI supply concept	HRS supply concept
Demand	4467 kWh/a (electric)	1380 t (H ₂)
Energy coverage [%]	20.4/43.8	100
Cost (annuities) [M€/a]	0.41	8.9
CO ₂ -eq. emissions [t/a]	1287	3730
PV peak power [MW]	0.38	25
Nominal wind power [MW]	4	19
Storage capacity	1172 kWh (electric)	46 t (H ₂)
Self-sufficiency [%]	76	100



(A): Energy demand, annuity, self-sufficiency, and PV peak power



(B): Wind power, storage capacity, CO₂-eq emissions, and coverage

FIGURE 9 | Comparative analysis of the OHLI and HRS supply concepts that lie at the center of the Pareto fronts. (A) Energy demand, annuity, self-sufficiency, and PV peak power. (B) Wind power, storage capacity, CO₂-eq emissions, and coverage.

Figure 9 compares a compromise solution for the OHLI and HRS supply concepts at the Gerolstein study site.

The HRS supply concept provides more energy to the respective multiple units than the OHLI one, as displayed in Figure 9A. On the one hand, this is caused by higher conversion losses of the

hydrogen–electric drive in comparison to the battery–electric one, leading to a higher energy demand for the HRS supply concept. On the other hand, the hydrogen path supplies all vehicles on the line with their entire energy demand; the OHLI path, meanwhile, supplies only a part of the total energy demand at the Gerolstein location (Figure 9B). Note that for the OHLI supply concept, two

different lines (see Figure 4) with different lengths are supplied with energy. Therefore, the share of energy differs between both lines. In the case study, there are existing overhead lines along the route that provide significant shares of the total energy demand for the OHLI supply concept. As this study examines a single location, the energy supply of overhead lines not located in Gerolstein are not considered.

The evaluations of Figure 9 show a comparative analysis of both supply concepts (OHLI and HRS). Due to the significantly higher energy demand of the HRS supply concept, the KPIs used for comparison were divided by the energy demand of the respective supply concept (MWh_d). Otherwise, the higher energy demand of the HRS supply concept scales optimization targets and KPIs. Only the self-sufficiency KPI is inherently adapted to the respective demand and, therefore, no division by the energy demand is carried out.

In the case of the HRS supply concept, significantly greater costs can be observed on a per supplied MWh basis. However, a direct comparison must account for several structural differences.

The OHLI supply concept is more flexible than the HRS one because the grid connection can be used to directly supply the BEMUs. In the case of the HRS supply concept, a grid connection is also integrated, but the electricity cannot be used to directly supply the HEMUs; the hydrogen must be produced via electrolysis and temporarily stored. This increases the system cost, as the hydrogen supply must also be ensured in corresponding quantities during extreme load times.

It can also be observed that the HRS supply concept produces lower CO_2 -eq emissions per GWh of electrical load required, compared to the OHLI supply concept.

Figure 9B shows the installed power of renewable generation based on wind and PV. The OHLI system relies primarily on wind energy, whereas the HRS supply system is mostly based on PV and wind with comparable power levels (peak power for PV and nominal power for wind) per supplied energy unit.

The HRS supply concept installs larger renewable power capacities, considering the greater total energy demand. Therefore, energy supply via the hydrogen path would have a significantly larger local space requirement.

The battery of the OHLI supply concept was installed with a capacity of 1172 kWh. The HRS supply concept utilizes hydrogen storage with a capacity of 46 t. Based on the lower heating value for hydrogen, the energy capacity of the hydrogen storage system is about 1.5 GWh, which is orders of magnitude larger than that of the battery. Therefore, the storage capacities differ significantly between both supply concepts, also if the different system scales are considered.

Another difference lies in the degree of self-sufficiency of the respective supply paths Figure 9A. In the case of the OHLI supply concept, 76% of the electricity demand is served by local generation, whereas in the case of the HRS supply concept, almost the entirety of the electricity demand is served by local generation.

3.4 | Discussion

The results indicate a cost advantage for the OHLI supply concept compared to the HRS one. However, the HRS supply concept achieves lower CO_2 -eq emissions in relation to the energy supplied. Furthermore, the HRS supply concept can supply the entire line at a single location, which is not the case for the OHLI supply concept, as in this case study.

This study looks at the energy supply aspect and optimizes the scalable components, whereby the grid connection is not an optimization variable. This is particularly important for the OHLI supply concept, as converters are required to supply traction current from the public grid, which imposes significant additional costs. These converters supply the contact wire with single-phase electrical energy at 15 kV and 16.7 Hz, which is fed from a public three-phase medium-voltage grid that is operated at 10–30 kV and 50 Hz. Especially electrolyzers can stress the local electricity grid and, if the electric power is sufficiently high, even have supra-regional effects [48]. In general, electrolyzers bigger than 10 MW have significant demands on the existing infrastructure. For these, it is particularly advantageous to utilize existing infrastructure, such as decommissioned power plants [49]. In [50], 200 \$/kW was used as grid connection cost. Assuming these costs, the annuity increase for the OHLI supply concept is 0.042 M\$/a (2.7 MW_{Peak}) and the cost increase for the HRS concept is 0.324 M\$/a (21 MW_{Ely}), assuming 1\$ = 0.92€. This cost always have to be considered in accordance to the local electricity grid situation. However, special electrolyzers are capable of changing their power in the order of milliseconds. Therefore, they can offer flexibility to the electricity system and thus generate revenue [51, 52].

In this study, the OHLI load time series was modeled in 10-min intervals. This does not describe the usual time interval for electricity trading, which is 15 min and was not critical in this studies, as a constant electricity price is assumed.

Performance degradation of batteries and fuel cells was not considered in this study. It was not included as these models significantly increase calculation time. For example [9], modeled battery aging for a 336 interval problem, resulting in 1200 s calculation time for each run. This paper uses weather data of 1 year. Therefore, the application of such details models is not possible. The integration of long-term storage and application of performance degradation models is thus interesting as a direction of future research.

This study is dependent on several sensitivities. First of all, 1 year was simulated to highlight seasonal dependencies. However, other weather years could change the system dimensions, as wind resources and solar irradiance vary from year to year.

Additionally, the results heavily depend on the parameterization. Grid-related CO_2 -eq emissions are assumed to be static over the period under consideration, which is not the case in reality [53]. System element costs are not uniform and decrease over time due to economies of scale and technological developments [10, 54]. Moreover, no distinction is made between WT and PVS feed-in tariffs, which implicitly assumes that there were no regulatory-based differences between WT or PVS in

this study. Calculation of Pareto fronts is computationally expensive. Therefore, it is usually performed using constant cost parameters, as in [55–57]. Changing parameters of the optimization does result in a shift of the Pareto front, but no significant change regarding the shape of the Pareto front [58]. Both supply concepts are significantly affected by the cost of PV and wind energy systems. In [59], capital cost for PV systems are 600–2794 \$/kW and wind onshore is 1039–3217 \$/kW in cost. This study considered 900 €/kW for PV and 1700 €/kW for wind. Therefore, the considered capital cost lies between the minimum and maximum values for both technologies. Furthermore, capital cost on a per kW basis for wind energy systems are higher than for PV systems. PV and wind energy systems reached the full commercialization phase [60]. The future cost for wind energy systems is expected to slow down [61]. However, the cost decrease in PV systems is expected to be higher than the cost decrease in wind energy systems. Therefore, designing a system at a future stage could shift towards a higher PV integration due to its respective cost reduction [62]. The battery cost is modeled on the basis of 430 €/kWh. In [63], a review on the battery cost in Germany is conducted. They stated the cost for medium cost battery systems (< 1000 kWh) between 580 and 710 €/kWh and the cost for large size battery systems (> 1000 kWh) between 310 and 465 €/kWh. The authors also stated a cost increase for battery systems from 2021 to 2022 highlighting the uncertainty of cost modeling. According to Mauler et al. [64], battery pack prices are to be expected to decrease by around 70% in 2050 compared to 2020. The electrolyzer was parameterized with a cost value of 636 €/kW. This lies in the range of PEM electrolyzers of 368–800 €/kW (400–870 \$/kW, assuming 1 \$ = 0.92 €). Future PEM electrolyzer prices are expected to decrease, where the current learning rate is 7–11% and the target learning rate is 13% [65]. The electricity cost and feed in tariffs are selected to current prices schemes for Germany. The electricity cost for industry increased from 15.32 €/kWh in 2014 to 16.65 €/kWh in 2024. However, the electricity cost exhibits significant variety as, for example, in 2022 the electricity cost reached 43.20 €/kWh [66]. The energy cost is especially relevant for the OHLI supply concept, as it relies to a higher degree on the public grid than the HRS supply concept. Furthermore, the feed in tariff significantly decreased by around 75% from 2009 to 2019 [13]. In general, feed in tariffs are an instrument of policymakers and thus are subject to change [67].

The discretization of WTs is an important factor in the case of the OHLI supply concept, as a clear division into stages can be seen. Therefore, a different discretization, due to other nominal wind power values of a single turbine, could influence the location of the stages. This factor is less significant for the PVS sizing, as the steps are in the kW range instead of the MW one that are used in the case of WTs. Another challenge is the integration of WTs in spatial proximity to the OHLI site. There are distance rules between WTs and residential areas that could prevent the construction of WTs. Furthermore, a sufficient free area must be available for erecting WTs or PVS.

The transport of hydrogen from the production site to the refueling station must be ensured and a redundant solution developed for potential operational disruptions (traffic obstructions, truck failure, and so on). This has a negative

impact on the overall costs. For example, a larger storage capacity must be planned for at the filling station site. These factors were not considered in the results presented in this study, however. If the hydrogen is not produced on-site, an average of approx. 3,800 kg of hydrogen per day have to be transported by trailer. This means that, on average, around four lorries per day from an H₂ production site to the HRS are required to keep the storage tanks full. If the deliveries cannot take place daily (e.g. on Sundays), the storage capacity on site must be expanded accordingly. This is currently around 11,500 kg and 20,000 kg. An expansion is possible with an impact on overall costs and emissions. The share of trailer supply in the total system costs of an off-site supply concept is approx. 15% and 0.02% of the CO₂-eq emissions. Furthermore, a pipeline system could be used for transport. In that case, the cost depends on pipeline material, required distance and pipe diameter [68].

4 | Conclusions and Outlook

This study investigates the supply of battery-electric multiple units (OHLI supply concept) and hydrogen-electric multiple units (HRS supply concept) at a single site (Gerolstein). The system configurations are described with Pareto fronts, where the optimization target variables are the costs and CO₂-eq emissions. Both supply concepts integrate renewable energy systems along the entire Pareto front. This shows that an integration of local generation is useful from both a cost point of view and to reduce CO₂-eq emissions. Comparing compromise system configurations (medium costs and medium CO₂-eq emissions), the OHLI supply concept is more cost-effective, whereas the HRS supply concept has lower CO₂-eq emissions per unit of energy provided. A structural difference is that the HRS supply concept provides the entire energy demand, whereas the OHLI supply concept does not. Thus, the absolute system size of the HRS supply concept is significantly larger at the site studied. A full supply from the OHLI supply concept would require more extensive system dimensioning. However, due to the island character of the energy supply concept, these systems would be located elsewhere, therefore not affecting the study's focus area of Gerolstein.

Further research should examine existing infrastructure and its costs for the OHLI supply concept. In the past, a falling trend in feed-in tariffs has been observed. However, the costs for renewables is also declining rapidly [69]. Therefore, the system's sizing for the future could lead to different outcomes. The effects of extreme weather phases are also a significant factor, especially for the HRS supply concept. Here, the purchase of hydrogen via trailers could potentially further reduce the costs. The upstream electricity grid is also not part of the study. An evaluation of the grid's repercussions is generally necessary but requires corresponding data.

This modeling approach, consisting of design and operational optimization, enables the evaluation of renewable energy integration in the transformation of non-electrified railway lines. It can therefore also be applied to other lines to find Pareto-optimal system configurations.

Acknowledgements

This study was funded by the German Center for Rail Traffic Research (DZSF) at the Federal Railway Authority (EBA), project No. EBA_2020-13-U-1202. Open Access funding enabled and organized by Projekt DEAL.

References

- DENA, *Non-Electrified Railway Transport* (2023), https://www.dena.de/fileadmin/dena/Publikationen/PDFs/2019/DENA-Factsheet_Rail_Transport_englisch.pdf.
- R. Thorne, A. H. Amundsen, and I. Sundvor, *Battery Electric and Fuel Cell Trains—Maturity of Technology and Market Status* (Oslo: Norwegian Centre for Transport Research, 2019).
- M. Handwerker, J. Wellnitz, and H. Marzbani, “Comparison of Hydrogen Powertrains With the Battery Powered Electric Vehicle and Investigation of Small-Scale Local Hydrogen Production Using Renewable Energy,” *Hydrogen* 2, no. 1 (2021): 76–100, <https://doi.org/10.3390/hydrogen2010005>.
- A. Hoffrichter, S. Hillmansen, and C. Roberts, “Conceptual Propulsion System Design for a Hydrogen-Powered Regional Train,” *IET Electrical Systems in Transportation* 6, no. 2 (2016): 56–66, <https://doi.org/10.1049/iet-est.2014.0049>.
- J. Pagenkopf, Toni Schirmer, M. Böhm, C. Streuling, and S. Herwartz, *Marktanalyse alternativer Antriebe im deutschen Schienenpersonennahverkehr* (DLR—Institut für Fahrzeugkonzept, 2020), https://elib.dlr.de/134615/1/DLR_2020_Marktanalyse%20alternative%20Antriebe%20SPNV.pdf.
- M. Böhm, A. Fernández Del Rey, J. Pagenkopf, M. Varela, S. Herwartz-Polster, and B. Nieto Calderón, “Review and Comparison of Worldwide Hydrogen Activities in the Rail Sector With Special Focus on On-Board Storage and Refueling Technologies,” *International Journal of Hydrogen Energy* 47, no. 89 (2022): 38003–38017, <https://doi.org/10.1016/j.ijhydene.2022.08.279>.
- F. C. Barbosa, *Battery Electric Rail Technology Review—A Technical and Operational Assessment. Current Status, Challenges and Perspectives* (2022), <https://doi.org/10.1115/JRC2022-78133>.
- C. Streuling, J. Pagenkopf, M. Schenker, and K. Lakeit, “Techno-Economic Assessment of Battery Electric Trains and Recharging Infrastructure Alternatives Integrating Adjacent Renewable Energy Sources,” *Sustainability* 13, no. 15 (2021): 8234, <https://doi.org/10.3390/su13158234>.
- A. Maheshwari, N. G. Paterakis, M. Santarelli, and M. Gibescu, “Optimizing the Operation of Energy Storage Using a Non-Linear Lithium-Ion Battery Degradation Model,” *Applied Energy* 261 (2020): 114360, <https://doi.org/10.1016/j.apenergy.2019.114360>.
- K. Mongird, V. Viswanathan, J. Alam, C. Vartanian, V. Sprenkl, and B. Richard, *2020 Grid Energy Storage Technology Cost and Performance Assessment* (Richland: U.S. Department of Energy, 2020).
- Y. Yang, Z. Wu, J. Yao, et al., “An Overview of Application-Oriented Multifunctional Large-Scale Stationary Battery and Hydrogen Hybrid Energy Storage System,” *Energy Reviews* 3, no. 2 (2024): 100068, <https://doi.org/10.1016/j.enrev.2024.100068>.
- K. Mongird, V. Viswanathan, P. Balducci, et al., “An Evaluation of Energy Storage Cost and Performance Characteristics,” *Energies* 13, no. 13 (2020): 3307, <https://doi.org/10.3390/en13133307>.
- J. Figgner, P. Stenzel, K. P. Kairies, et al., “The Development of Stationary Battery Storage Systems in Germany—A Market Review,” *Journal of Energy Storage* 29 (2020): 101153, <https://doi.org/10.1016/j.est.2019.101153>.
- N. Sazali, W. N. Wan Salleh, A. S. Jamaludin, and M. N. Mhd Razali, “New Perspectives on Fuel Cell Technology: A Brief Review,” *Membranes* 10, no. 5 (2020): 99, <https://doi.org/10.3390/membranes10050099>.
- V. Cigolotti, M. Genovese, and P. Fragiaco, “Comprehensive Review on Fuel Cell Technology for Stationary Applications as Sustainable and Efficient Poly-Generation Energy Systems,” *Energies* 14, no. 16 (2021): 4963, <https://doi.org/10.3390/en14164963>.
- R. Guo, Q. Li, and N. Zhao, “An Overview of Grid-Connected Fuel Cell System for Grid Support,” *Energy Reports* 8 (2022): 884–892, <https://doi.org/10.1016/j.egy.2022.05.211>.
- M. A. Abdelkareem, K. Elsaid, T. Wilberforce, M. Kamil, E. T. Sayed, and A. Olabi, “Environmental Aspects of Fuel Cells: A Review,” *Science of the Total Environment* 752 (2021): 141803, <https://doi.org/10.1016/j.scitotenv.2020.141803>.
- J.-N. Kang, Y.-M. Wei, L.-C. Liu, R. Han, B.-Y. Yu, and J.-W. Wang, “Energy Systems for Climate Change Mitigation: A Systematic Review,” *Applied Energy* 263 (2020): 114602, <https://doi.org/10.1016/j.apenergy.2020.114602>.
- C. Ammari, D. Belatrache, B. Touhami, and S. Makhloufi, “Sizing, Optimization, Control and Energy Management of Hybrid Renewable Energy System—A Review,” *Energy and Built Environment* 3, no. 4 (2022): 399–411, 2022/10/01/, <https://doi.org/10.1016/j.enbenv.2021.04.002>.
- R. Knibbe, D. Harding, E. Cooper, et al., “Application and Limitations of Batteries and Hydrogen in Heavy Haul Rail Using Australian Case Studies,” *Journal of Energy Storage* 56 (2022): 105813, <https://doi.org/10.1016/j.est.2022.105813>.
- S. Herwartz, J. Pagenkopf, and C. Streuling, “Sector Coupling Potential of Wind-Based Hydrogen Production and Fuel Cell Train Operation in Regional Rail Transport in Berlin and Brandenburg,” *International Journal of Hydrogen Energy* 46, no. 57 (2021): 29597–29615, <https://doi.org/10.1016/j.ijhydene.2020.11.242>.
- D. Sadeghi, N. Amiri, M. Marzband, A. Abusorrah, and K. Sedraoui, “Optimal Sizing of Hybrid Renewable Energy Systems By Considering Power Sharing and Electric Vehicles,” *International Journal of Energy Research* 46, no. 6 (2022): 8288–8312, <https://doi.org/10.1002/er.7729>.
- L. Schmeling, P. Schönfeldt, P. Klement, et al., “A Generalised Optimal Design Methodology for Distributed Energy Systems,” *Renewable Energy* 200 (2022): 1223–1239, <https://doi.org/10.1016/j.renene.2022.10.029>.
- A. M. Hemeida, A. S. Omer, A. M. Bahaa-Eldin, et al., “Multi-Objective Multi-Verse Optimization of Renewable Energy Sources-Based Micro-Grid System: Real Case,” *Ain Shams Engineering Journal* 13, no. 1 (2022): 101543, <https://doi.org/10.1016/j.asej.2021.06.028>.
- statista. Strompreise für die Industrie in Deutschland bis 2020, 2024, <https://de.statista.com/statistik/daten/studie/155964/umfrage/entwicklung-der-industriestrompreise-in-deutschland-seit-1995/>.
- Bundesnetzagentur. Ergebnisse der Ausschreibungen für Windenergie 2021, 2022, https://www.bundesnetzagentur.de/DE/Sachgebiete/ElektrizitaetundGas/Unternehmen_Institutionen/Ausschreibungen/Wind_Onshore/BeendeteAusschreibungen/BeendeteAusschreibungen_node.html.
- Bundesnetzagentur. Anzulegende Werte für Solaranlagen, 2022, https://www.bundesnetzagentur.de/SharedDocs/Downloads/DE/Sachgebiete/Energie/Unternehmen_Institutionen/ErneuerbareEnergien/ZahlenDatenInformationen/PV_Datenmeldungen/DegressionsVergSaetze_02bis0422.xlsx?__blob=publicationFile&v=2.
- Bundesnetzagentur. Ergebnisse der Ausschreibungsrunden für Solar-Anlagen 2021, 2022, <https://www.bundesnetzagentur.de/DE/Fachthemen/ElektrizitaetundGas/Ausschreibungen/Solaranlagen1/BeendeteAusschreibungen/start.html>.
- C. Kost, S. Shammugam, V. Fluri, D. Peper, A. D. Memar, and T. Schlegl, *Levelized Cost of Electricity Renewable Energy Technologies* (Freiburg: Fraunhofer Institute for Solar Energy Systems ISE, 2021).
- RLI, *Smooth GitHub Repository*. Berlin, <https://github.com/rl-institut/smooth>.
- C. Olalla, D. Maksimovic, C. Deline, and L. Martinez-Salamero, “Impact of Distributed Power Electronics on the Lifetime and Reliability of PV

- Systems,” *Progress in Photovoltaics: Research and Applications* 25, no. 10 (2017): 821–835, <https://doi.org/10.1002/pip.2893>.
32. International Electrotechnical Commission, *IEC 61400-Wind Turbines—Part 1: Design Requirements* (2005).
33. T. Bruckner, et al., “Energy Systems. Climate Change 2014: Mitigation of Climate Change. Contribution of Working Group III to the Fifth Assessment Report of the Intergovernmental Panel on Climate Change,” pp. 511–598 (2014), <https://doi.org/10.1017/CBO9781107415416.013>.
34. J. P. Manuel Baumann and Marcel Weil, “Ökologische und ökonomische Performance stationärer Li-Ion-Batteriespeicher,” presented at the 15. Symposium Energieinnovation, Technische Universität Graz, 14. bis 16. February, 2018.
35. Umweltbundesamt. Entwicklung der spezifischen Kohlendioxid-Emissionen des deutschen Strommix in den Jahren 1990–2020, 2021, https://www.umweltbundesamt.de/sites/default/files/medien/5750/publikationen/2021-05-26_cc-45-2021_strommix_2021.pdf.
36. J. Burkhardt, A. Patyk, P. Tanguy, and C. Retzke, “Hydrogen Mobility From Wind Energy—A Life Cycle Assessment Focusing on the Fuel Supply,” *Applied Energy* 181 (2016): 54–64, <https://doi.org/10.1016/j.apenergy.2016.07.104>.
37. S. Hilpert, C. Kaldemeyer, U. Krien, S. Günther, C. Wingenbach, and G. Plessmann, “The Open Energy Modelling Framework (oemof)—A New Approach to Facilitate Open Science in Energy System Modelling,” *Energy Strategy Reviews* 22 (2018): 16–25, <https://doi.org/10.1016/j.esr.2018.07.001>.
38. g. R. GmbH. *Public Transport Authority* (2021), <https://wir.gorheinland.com/angebot/liniennetz/>.
39. C. Streuling, S. Arens, M. Schenker, and J. Pagenkopf, “Potentialanalyse der BEMU-Nachladung mittels Direktstromnutzung aus EEA,” *Elektrische Bahnen* 121, no. 9 (2023): 310–321.
40. A. Bomhauer-Beins, S. Schranil, and U. Weidmann, “Einflüsse auf den Bahnenergiebedarf und iesbezügliche Potentiale der Automatisierung,” *Schweizer Eisenbahn-Revue*, no. 3 (2018): 140–144.
41. Deutscher Wetterdienst, *Zeitreihen fuer Gebietsmittel fuer Bundeslaender und Kombinationen von Bundeslaender* (Berlin: Beuth-Verlag, 2022), https://opendata.dwd.de/climate_environment/CDC/regional_averages_DE/monthly/air_temperature_mean/.
42. German Institute for Standardization, *DIN EN 50367* (2017).
43. Deutscher Bundestag. “Sicherstellung der Stromversorgung bei Dunkelflauten,” 2019, accessed May 25, 2022, <https://www.bundestag.de/resource/blob/627898/b65deea51fdb399e4b64f1182465658d/WD-5-167-18-pdf-data.pdf>.
44. RLI. *Open Feed-In Time Series Based on a Renewable Energy Database*, 2019, <https://github.com/open-fred>.
45. oemof Entwicklungsteam, *windpowerlib*, 2017, <https://github.com/wind-python/windpowerlib>.
46. W. F. Holmgren, C. W. Hansen, and M. A. Mikofski, “Pvlib Python: S Python Package for Modeling Solar Energy Systems,” *Journal of Open Source Software* 3 (2018): 884, <https://doi.org/10.21105/joss.00884>.
47. A. S. Rana, M. Nasir, and H. A. Khan, “String Level Optimisation on Grid-Tied Solar Pv Systems to Reduce Partial Shading Loss,” *IET Renewable Power Generation* 12, no. 2 (2018): 143–148, <https://doi.org/10.1049/iet-rpg.2017.0229>.
48. J. Bartels, C. Varela, T. Wassermann, W. Medjroubi, and E. Zondervan, “Integration of Water Electrolysis Facilities in Power Grids: A Case Study in Northern Germany,” *Energy Conversion and Management: X* 14 (2022): 100209, <https://doi.org/10.1016/j.ecmx.2022.100209>.
49. A.-K. Klaas, M. Diehl, N. Fadl, M. Moritz, and L. Reste, *Standortbewertung für systemdienliche Elektrolyseure—eine regionale Analyse Multipler Einflussfaktoren* (Energiewirtschaftliches Institut an der Universität zu Köln gGmbH (EWI), 2024), https://www.ewi.uni-koeln.de/cms/wp-content/uploads/2024/07/20240712_EWI_EON_Thuega_Abschlussbericht_final.pdf.
50. T. Nguyen, Z. Abdin, T. Holm, and W. Mérida, “Grid-Connected Hydrogen Production Via Large-Scale Water Electrolysis,” *Energy Conversion and Management* 200 (2019): 112108, <https://doi.org/10.1016/j.enconman.2019.112108>.
51. J. Eichman, K. Harrison, and M. Peters, *Novel Electrolyzer Applications: Providing More Than Just Hydrogen* (2014), <https://doi.org/10.2172/1159377>.
52. E. Stamatakis, E. Perwög, E. Garyfallos, M. S. Millán, E. Zoulias, and N. Chalkiadakis, “Hydrogen in Grid Balancing: The European Market Potential for Pressurized Alkaline Electrolyzers,” *Energies* 15, no. 2 (2022): 637, <https://doi.org/10.3390/en15020637>.
53. EUPD Research *CO2-Emissionen im deutschen Strommix schwanken im Jahresverlauf 2020 sehr stark*, 2021, <https://www.eupd-research.com/co2-emissionen-im-deutschen-strommix-schwanken-im-jahresverlauf-2020-sehr-stark/>.
54. E. Williams1647, E. Hittinger, R. Carvalho, and R. Williams, “Wind Power Costs Expected to Decrease Due to Technological Progress,” *Energy Policy* 106 (2017): 427–435, <https://doi.org/10.1016/j.enpol.2017.03.032>.
55. R. Cheraghi and M. Hossein Jahangir, “Multi-Objective Optimization of a Hybrid Renewable Energy System Supplying a Residential Building Using NSGA-II and MOPSO Algorithms,” *Energy Conversion and Management* 294 (2023): 117515, <https://doi.org/10.1016/j.enconman.2023.117515>.
56. X. Yang, Z. Chen, X. Huang, R. Li, S. Xu, and C. Yang, “Robust Capacity Optimization Methods for Integrated Energy Systems Considering Demand Response and Thermal Comfort,” *Energy* 221 (2021): 119727, <https://doi.org/10.1016/j.energy.2020.119727>.
57. S. M. Alirahmi and E. Assareh, “Energy, Exergy, and Exergoeconomics (3E) Analysis and Multi-Objective Optimization of a Multi-Generation Energy System for Day and Night Time Power Generation—Case Study: Dezful City,” *International Journal of Hydrogen Energy* 45, no. 56 (2020): 31555–31573, <https://doi.org/10.1016/j.ijhydene.2020.08.160>.
58. J. Finke and V. Bertsch, “Implementing a Highly Adaptable Method for the Multi-Objective Optimisation of Energy Systems,” *Applied Energy* 332 (2023): 120521, <https://doi.org/10.1016/j.apenergy.2022.120521>.
59. G. R. Timilsina, “Are Renewable Energy Technologies Cost Competitive for Electricity Generation?,” *Renewable Energy* 180 (2021): 658–672, <https://doi.org/10.1016/j.renene.2021.08.088>.
60. A. Elia, M. Kamidelivand, F. Rogan, and B. Ó Gallachóir, “Impacts of Innovation on Renewable Energy Technology Cost Reductions,” *Renewable and Sustainable Energy Reviews* 138 (2021): 110488, <https://doi.org/10.1016/j.rser.2020.110488>.
61. P. Beiter, A. Cooperman, E. Lantz, et al., “Wind Power Costs Driven by Innovation and Experience With Further Reductions on the Horizon,” *WIREs Energy and Environment* 10, no. 5 (2021): e398, <https://doi.org/10.1002/wene.398>.
62. L. Sens, U. Neuling, and M. Kaltschmitt, “Capital Expenditure and Levelized Cost of Electricity of Photovoltaic Plants and Wind Turbines – Development by 2050,” *Renewable Energy* 185 (2022): 525–537, <https://doi.org/10.1016/j.renene.2021.12.042>.
63. J. Figgenger, et al., *The Development of Battery Storage Systems in Germany: A Market Review (Status 2023)*, arXiv, (2023), <https://doi.org/10.48550/arXiv.2203.06762>.
64. L. Mauler, F. Duffner, W. G. Zeier, and J. Leker, “Battery Cost Forecasting: A Review of Methods and Results With an Outlook to 2050,” *Energy & Environmental Science* 14, no. 9 (2021): 4712–4739, <https://doi.org/10.1039/D1EE01530C>.
65. A. Patonia and R. Poudineh, *Cost-Competitive Green Hydrogen: How to Lower the Cost of Electrolysers in OIES Paper: EL 47* (Oxford Institute for Energy Studies, 2022), <https://www.oxfordenergy.org/wpcms/wp-content/uploads/2022/01/Cost-competitive-green-hydrogen-how-to-lower-the-cost-of-electrolysers-EL47.pdf>.

66. BDEW. *BDEW-Strompreisanalyse Juli 2024* (2024), https://www.bdew.de/media/documents/240703_BDEW-Strompreisanalyse_Juli_2024_Korrektur.pdf.
67. Y. Karneyeva and R. Wüstenhagen, “Solar Feed-In Tariffs in a Post-Grid Parity World: The Role of Risk, Investor Diversity and Business Models,” *Energy Policy* 106 (2017): 445–456, 2017/07/01/, <https://doi.org/10.1016/j.enpol.2017.04.005>.
68. H. Lee and S. Lee, “Economic Analysis on Hydrogen Pipeline Infrastructure Establishment Scenarios: Case Study of South Korea,” *Energies* 15, no. 18 (2022): 6824, <https://doi.org/10.3390/en15186824>.
69. M. Xiao, T. Junne, J. Haas, and M. Klein, “Plummeting Costs of Renewables—Are Energy Scenarios Lagging?,” *Energy Strategy Reviews* 35 (2021): 100636, <https://doi.org/10.1016/j.esr.2021.100636>.